Article

pubs.acs.org/Biomac

Tough Coating Proteins: Subtle Sequence Variation Modulates Cohesion

Saurabh Das,[†] Dusty R. Miller,[‡] Yair Kaufman,[†] Nadine R. Martinez Rodriguez,[§] Alessia Pallaoro,[∥] Matthew J. Harrington,[⊥] Maryte Gylys,[∥] Jacob N. Israelachvili,*[,†,#] and J. Herbert Waite*[,‡,§,∥,#]

[†]Department of Chemical Engineering, [‡]Biomolecular Science and Engineering, [§]Department of Molecular, Cell and Developmental Biology, [∥]Department of Chemistry and Biochemistry, and [#]Materials Research Laboratory, University of California, Santa Barbara, California 93106, United States

[⊥]Department of Biomaterials, Max Planck Institute for Colloids and Interfaces, 14424 Potsdam-Golm, Germany

Supporting Information

ABSTRACT: Mussel foot protein-1 (mfp-1) is an essential constituent of the protective cuticle covering all exposed portions of the byssus (plaque and the thread) that marine mussels use to attach to intertidal rocks. The reversible complexation of Fe^{3+} by the 3,4-dihydroxyphenylalanine (Dopa) side chains in mfp-1 in *Mytilus californianus* cuticle is responsible for its high extensibility (120%) as well as its stiffness (2 GPa) due to the formation of sacrificial bonds that help to dissipate energy and avoid accumulation of stresses in the material. We have investigated the interactions between Fe^{3+} and mfp-1 from two mussel species, *M. californianus* (*Mc*) and *M. edulis* (*Me*), using both surface sensitive and solution phase techniques. Our results show that although mfp-1 homologues from both species bind Fe^{3+}, mfp-1 (*Mc*) contains Dopa with two distinct Fe^{3+}-binding tendencies and prefers to form intramolecular complexes with Fe^{3+}. In contrast, mfp-1 (*Me*) is better adapted to intermolecular Fe^{3+} binding by Dopa. Addition of Fe^{3+} did not significantly increase the cohesion energy between the mfp-1 (*Mc*) films at pH 5.5. However, iron appears to stabilize the cohesive bridging of mfp-1 (*Mc*) films at the physiologically relevant pH of 7.5, where most other mfps lose their ability to adhere reversibly. Understanding the molecular mechanisms underpinning the capacity of *M. californianus* cuticle to withstand twice the strain of *M. edulis* cuticle is important for engineering of tunable strain tolerant composite coatings for biomedical applications.

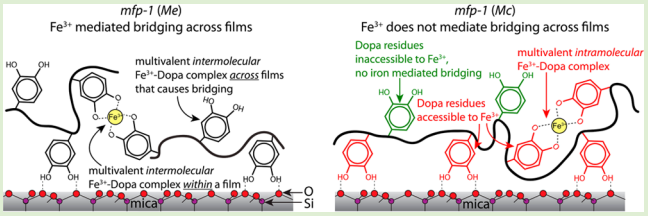

INTRODUCTION

Protective coatings are used in manufacturing to improve the abrasion, scratch, corrosion, and ultraviolet-light resistance of target surfaces and thereby adds significantly to product performance and value. Current coating applications based on polymers are limited by the high modulus/low strain (epoxies) or low modulus/high strain (polyurethanes) of available polymers,[1−3] but could be significantly diversified with polymers that were both stiff and extensible. Natural composite coatings of marine mussels involve prefabrication of granules and matrix in secretory cells of the accessory gland located in the foot. During thread formation, the granule/matrix blend is released over the collagenous thread core in a process similar to injection molding. Upon equilibration with seawater, the blend matures into a hard coating cross-linked by coordination with Fe^{3+} complexes.[4−6] The naturally occurring polymeric coatings of mussel byssus have a modulus of 2 GPa and strains of about 75 and 120% in *Mytilus galloprovincialis* (*Mg*)[4] and *Mytilus californianus* (*Mc*),[5,6] respectively, making them among the most energy tolerant coatings known.[3] Previous characterizations of byssal coatings have detected Fe^{3+} and a 3,4-dihydroxyphenylalanine (Dopa)-containing protein known as mussel foot protein 1 (mfp-1).[7,8] Resonance Raman microscopy indicates that Fe^{3+} and Dopa are coupled as tris-catecholato−Fe^{3+} complexes in the coatings and are proposed to provide reversible protein cross-links between mfp-1 proteins.[6] This cross-linking has been recapitulated in vitro in mixtures of isolated mfp-1 and Fe^{3+}[9] and increases the stiffness of mfp-1 gels.[10] Similar results were obtained with synthetic and natural catechol-functionalized polymers and Fe^{3+}[11−13] and metal cations.[14] More recently, Dopa−Fe^{3+} complexes were proposed to contribute to the strong and reversible iron-dependent cohesion energy (~4 mJ/m^2) between two monolayers of mfp-1 from *M. edulis*.[15]

Homologous proteins from closely related species often provide unique opportunities for gaining mechanistic insights into structure−function relationships as well as biochemical adaptations to the environment.[16,17] In this spirit, we investigated the cohesive and adhesive properties of an mfp-1 homologue from a related mussel, *M. californianus* (*Mc*), whose byssal coating has an ultimate strain in excess of 120%[4,5] and also contains Dopa−Fe^{3+} complexes. Mfp-1 from both species consists of tandem decapeptide repeats: the consensus decapeptide PKISYP**P*TY*K (where P*, P**, and Y*

Received: December 27, 2014
Revised: February 10, 2015
Published: February 18, 2015

DOI: 10.1021/bm501893y
Biomacromolecules 2015, 16, 1002−1008

denote *trans*-4-hydroxyproline, dihydroxyproline, and Dopa, respectively) in *Mc* is highly similar to AKPSYP**P*TY*K in *Me* and *Mg*;[18,19] indeed, apart from the inverted order of the first three amino acids, the only net change is an A → I substitution. A preliminary study of cohesion in two symmetric *Mc* mfp-1 monolayers using the surfaces forces apparatus (SFA) showed significantly greater intrinsic cohesion than its homologue from *Me* (cohesion energy, $W_c \sim 1.7-3.4$ mJ/m^2 in *Mc* vs $W_c \sim 0$ in *Me*[20]). Given the prominence of mfp-1 and iron in the composite structure of byssal cuticle, we investigated the protein and Fe^{3+} concentration-dependent cohesion of mfp-1 at different pH values. Despite their similar sequences, mfp-1 (*Mc*) and mfp-1 (*Me*) films exhibit strikingly different cohesive properties with and without Fe^{3+} in the surface forces apparatus. Understanding these differences will help inspire the design of future biomimetic polymers or recombinant mfp-1 proteins for biomedical and functional coatings for wet adhesion and friction applications.[21−25]

EXPERIMENTAL SECTION

Purification of Mfp-1 (*Mc* and *Me*). Mfp-1 was purified as described previously[26] with some modifications. Briefly, flash frozen *Me* mussel feet were provided by NorthEast Transport (Waldoboro, Me, U.S.A.). *Mc* mussels were collected from Goleta Pier, (Santa Barbara, CA), and held in circulation tanks. The mussels were shucked and the foot was severed from the body and frozen to −70 °C before fileting off the pigmented epithelium. Approximately 50 prepared feet of Mc or Me were homogenized in four equivalents (w/v) of 5% acetic acid (v/v), 10 μM leupeptin, 10 μM pepstatin, and 1 mM EDTA in a glass Kontes tissue grinder (Vineland, NJ) on ice and centrifuged at 20000 × *g*, 4 °C for 40 min. The supernatant was acidified with 70% perchloric acid to a final concentration of 1.5% (v/v). After centrifugation at 20000 × *g*, 4 °C for 40 min, the supernatant was dialyzed 4 × 4 L of 5% acetic acid (v/v) for ≥4 h with 1000 kDa molecular weight cutoff dialysis tubing (Spectrum Industries, Los Angeles, CA) before freeze-drying. The lyophilized protein was resuspended in 200 μL of 5% acetic acid (v/v) and 50 μL aliquots were run over a Shodex KW-803 size exclusion column (5 μm, 8 × 300 mm; New York, NY). Fractions were monitored at 280 nm and those positive for protein were subjected to acid-urea polyacrylamide gel electrophoresis (7.5% acrylamide and 0.2% *N*,*N*-methylenebis-(acrylamide)) containing 5% acetic acid and 8 M urea.[27] After electrophoresis, gels were stained with Sigma-Aldrich Coomassie Blue R-250 (Brooklyn, NY). Pure mfp-1 fractions were pooled and aliquoted before freeze-drying and stored at −70 °C for future use.

To avoid confusion about the mussel species referred to, namely, *Mytilus californianus*, *M. edulis*, and *M. galloprovincialis*, the following clarification is added: *Mytilus californianus* is a distinct species. However, *M. edulis*, with *M. trossulus* and *M. galloprovincialis*, is one of three subspecies of the well-known *Mytilus* complex. The three species are genetically distinguishable at only one known genetic locus,[28] interbreed, and have viable hybrid offspring.[29,30] Mfp-1 in the 3 species consists mostly of tandemly repeated AKPSYPPTYK sequences.[28] Given these, we have assumed that the cuticle properties of *Mytilus* complex species are indistinguishable. Indeed, an earlier study also concluded this for the mechanical properties of byssal threads from *Mytilus* complex species.[31]

Measuring the Adhesive/Cohesive Interactions. The surface forces apparatus (SFA, SurForce LLC) was used to measure the normal forces between two mica surfaces in a cross-cylindrical geometry (glued onto two cylindrical glass surfaces with Epoxy EPON Resin 1004F glue) as a function of the separation distance, *D*, between them and has been described elsewhere.[32,33] Mfp-1 (*Mc*) films were made by adsorbing 50 μL of the protein from a C_{fp1} = 10−100 μg/mL in a buffer solution (0.1 M sodium acetate buffer, pH 5.5, 0.25 M KNO_3, and 1 mM bis−tris) onto the mica surfaces for 30 min, then rinsing the excess protein with the same buffer. During the protein adsorption, the discs were kept in a saturated Petri dish to minimize evaporation of the water from the surfaces. The discs were then mounted in the SFA in one of two configurations. In an asymmetric configuration (Figure S3), the mussel protein was adsorbed on one surface in order to measure the interaction (*adhesion*) between the mfp-1 (*Mc*) film and the mica surface.

In a symmetric configuration (Figure 1), the mussel protein film was deposited on both surfaces in order to measure *cohesion* between the protein films. Cohesion was tested with and without iron. Iron solutions 1, 10, 100 μM $FeCl_3$ in acetate buffer (as above) were freshly made and added to the symmetrically deposited protein by injection of progressively higher concentrations of Fe^{3+} between the surfaces. The pH of the solution between the surfaces was increased to 7.5 by rinsing with a phosphate buffer (0.1 M potassium phosphate, pH 7.5, 0.25 M KNO_3).

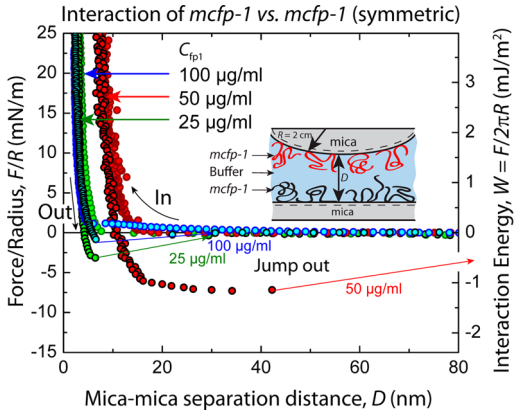

Figure 1. Cohesion between two symmetric mfp-1 (*Mc*) films. Representative force vs distance plots for mfp-1 (*Mc*) films at three protein concentrations (C_{fp1} = 25, 50, and 100 μg/mL in 0.1 M sodium acetate buffer, pH 5.5, 0.25 M KNO_3, and 1 mM bis−tris).

The protein films were always hydrated (i.e., never allowed to dry) and a droplet of the acetate buffer was injected between the surfaces immediately after loading in the SFA. During a typical approach-separation force measurement cycle, the surfaces were first moved toward each other (approach) until reaching a "hardwall" and then separated. The hardwall distance is the separation distance between the two mica surfaces upon compression that does not change with increased compression. The energy of interaction between two crossed-cylinder geometry, roughly corresponds to a sphere of radius *R* approaching a flat surface based on the Derjaguin approximation, $W(D) = F(D)/2\pi R$, where $W(D)$ is the energy of interaction per unit area between two flat surfaces and $F(D)$ is the measured force of interaction in the SFA. The measured adhesion (or cohesion) force F_{ad} (or F_c) is related to the adhesion (or cohesion) energy per unit area by $W_{ad} = F_{ad}/2\pi R$ for rigid surfaces with weak adhesive interactions and by $W_{ad} = F_{ad}/1.5\pi R$ (used in this study) for soft deformable surfaces with strong adhesion or cohesion.[34,35]

AFM Imaging Proteins at the Interface. Images were acquired using MFP-3D-Bio Atomic Force Microscope (AFM, Asylum Research) using SNL (Sharp Nitride Lever) probe (Bruker) in tapping mode at room temperature (22 °C). Mfp-1 (*Mc*) was deposited on a mica surface (area ∼ 1 cm^2) by adsorbing 50 μL of the protein from a 10, 25, 50, and 100 μg/mL in the buffer solution at pH 5.5. The protein film roughness was obtained by analyzing the AFM image using the software Gwyddion v.2.36 and has been described previously.[22]

Cyclic Voltammetry (CV). The CV measurements were performed using a three electrode electrochemical setup consisting of a carbon paste working electrode (WE), platinum counter electrode (CE), and a AglAgCl (3 N KCl) reference electrode (RE) and has been described elsewhere.[36] The electrochemical potential was controlled using a Gamry potentiostat (Reference 600 Series). A

DOI: 10.1021/bm501893y
Biomacromolecules 2015, 16, 1002−1008

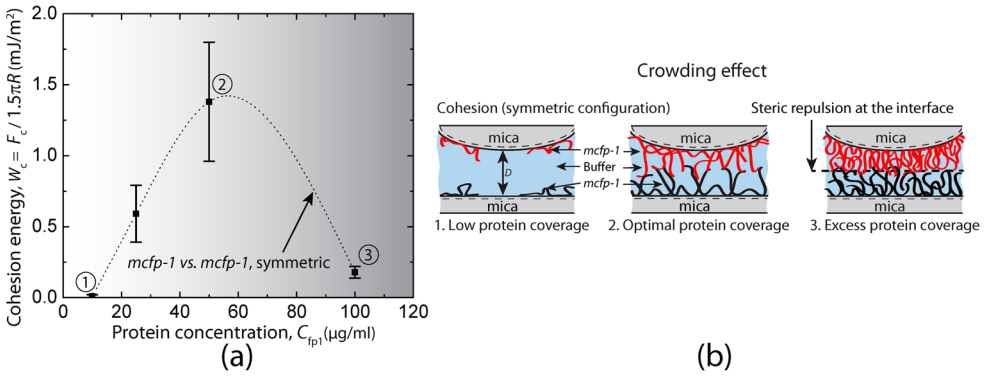

Figure 2. Concentration-dependence of cohesion between two symmetric mfp-1 (*Mc*) films. (a) Effect of protein deposition concentration on the cohesion (mfp-1 (*Mc*) vs mfp-1 (*Mc*), symmetric) energies of interaction between the surfaces. (b) Schematic representations of the crowding effect for cohesion. For clarity, the protein molecules on the upper and lower mica surfaces are shown in red and black colors, respectively.

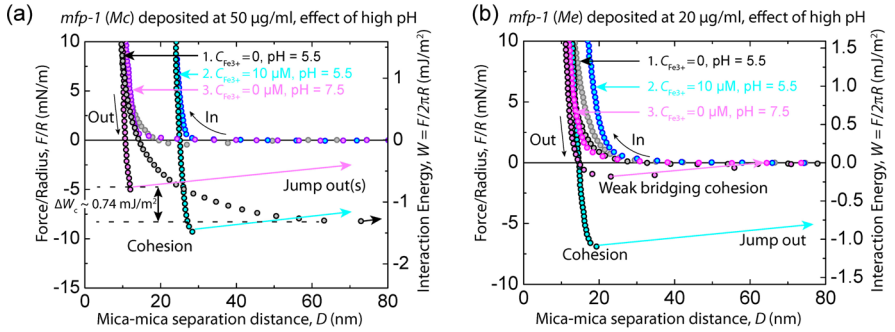

Figure 3. pH dependence of Fe^{3+}-mediated cohesion between two symmetric mfp-1 (*Mc*) films. Representative force vs distance plot showing the interaction between two symmetric mfp-1 (*Mc*) films deposited at 50 μg/mL in 0.1 M sodium acetate buffer, pH 5.5, 0.25 M KNO_3, and 1 mM bis-tris with $C_{Fe^{3+}}$ = 0 (gray) and 100 μM (blue) at pH 5.5. The cohesion between the mfp-1 (*Mc*) films was preserved after increasing the pH to 7.5 (magenta). (b) Representative force vs distance plot showing the interaction between two symmetric mfp-1(*Me*) films deposited at 20 μg/mL in 0.1 M sodium acetate buffer, pH 5.5, 0.25 M KNO_3, and 1 mM bis−tris with $C_{Fe^{3+}}$ = 0 (gray) and 100 μM (blue) at pH 5.5. The surfaces showed a weak bridging cohesion (W_c < 0.2 mJ/m²) after increasing the pH to 7.5 (magenta). It should be noted that $C_{Fe^{3+}}$ is the concentration of ferric cation in the bulk solution between the surfaces. Flushing with buffer at pH 7.5 removes iron from the bulk solution, however, to the extent that the preadsorbed protein films already had some bound Fe^{3+}, the Dopa−Fe^{3+} complexes will be present in them.

total of 5 μL of 50 μg/mL of the mfp-1 (*Mc*; or 10 μL of 20−100 μg/mL mfp-1 (*Me*) was dissolved in 1 mL buffer solution (10 mM NaCl and pH 3.7) and a triangular wave potential sweep was applied on the WE between chosen negative and positive limits and the cycle was repeated three times from measuring CV profiles. Higher concentrations of mfp-1 (*Me*) were used for the measurements to get a Dopa oxidation current peak similar or more than the mfp-1 (*Mc*). This strategy provides a better understanding of the Dopa−Fe complexation mechanism in the proteins and has been discussed in the results and discussion sections. The measurements were also done in the buffer solution with 10 μM Fe^{3+} to test the effect of ferric ions on the oxidation behavior of the proteins.

RESULTS

Cohesive Interactions between the mfp-1 (*Mc*) Films. The first challenge in any study involving surface forces between symmetric films is to optimize protein concentrations for film deposition. The cohesion between two symmetrically deposited mfp-1 (*Mc*) films on the mica surfaces was measured using the SFA (symmetric system, see Figure 1). Protein deposition from a solution concentration of C_{fp1} = 10 μg/mL resulted in no attraction between the protein films. Increasing the protein solution concentration to 25 μg/mL resulted in a cohesion energy of W_c = 0.59 ± 0.20 mJ/m² between the films (Figure 2). A further increase to 50 μg/mL doubled the cohesion (W_c = 1.24 ± 0.40 mJ/m²). At C_{fp1} = 100 μg/mL, cohesion decreased significantly to W_c = 0.18 ± 0.04 mJ/m² (Figure 2). The surfaces exhibited poor bridging *cohesion*[32] at C_{fp1} = 25 and 100 μg/mL compared with mfp-1 (*Mc*) bridging at C_{fp1} ~ 50 μg/mL (Figure 1).

Interestingly, addition of Fe^{3+} did not change the cohesion force measured between the mfp-1 (*Mc*) films significantly for $C_{Fe^{3+}}$ = 0−100 μM (Figure S1). These results are in stark contrast to the behavior of mfp-1 (*Me*), a homologue from *M. edulis*, where at pH 5.5, 10 μM Fe^{3+} caused two noninteracting mfp-1 (*Me*) protein films to bridge.[15] In any given experiment, Fe^{3+} expanded the mfp-1 (*Mc*) film on the mica surface progressively with increasing $C_{Fe^{3+}}$. The thickness of the mfp-1 (*Mc*) film deposited at 50 μg/mL increased from 8.5 to 15 nm between $C_{Fe^{3+}}$ = 0 and 100 μM, respectively (Figure S1).

Addition of Fe^{3+} has a peculiar effect on cohesion between the protein films even after increasing the pH of the solution to 7.5 (Figure 3). Previous studies of a variety of mfps have reported a short-term cohesion loss that was attributed to the oxidation of Dopa to Dopa−quinone,[37−39] but these were done without added Fe^{3+}. With mfp-1 (*Mc*) alone, cohesion at pH 5.5 was robust (W_c ~ 1.4 mJ/m²) with a gradually increasing separation force. Addition of Fe^{3+} at pH 5.5 expanded the mfp-1 films from 8 to about 15 nm and stiffened them without changing the cohesion energy. This is consistent with extensive monocomplexation of Fe^{3+}, leading to mfp-1 (*Mc*) film

DOI: 10.1021/bm501893y
Biomacromolecules 2015, 16, 1002−1008

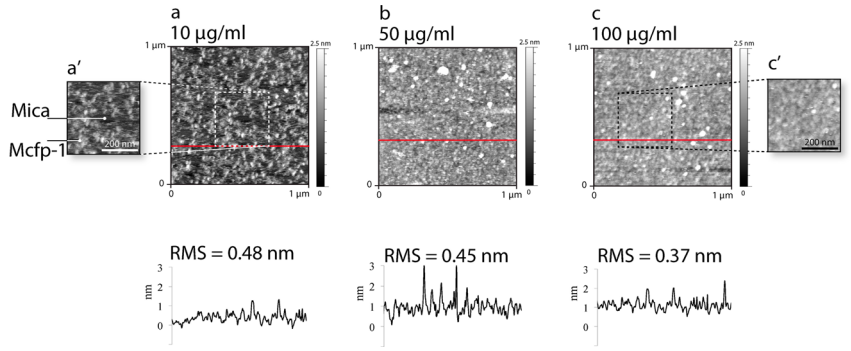

Figure 4. Mfp-1 (*Mc*) films adsorbed to mica. AFM topography images and their respective cross sections (below) showing the RMS roughness of mfp-1 (*Mc*) films on mica in pH 5.5 acetate buffer at different C_{fp1} = (a) 10, (b) 50, and (c) 100 μg/mL.

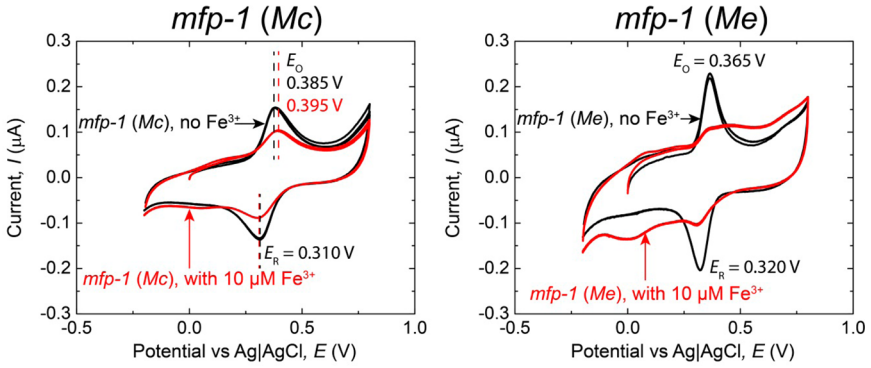

Figure 5. Cyclic voltammograms of mfp-1 (*Mc*) and mfp-1 (*Me*) with and without 10 μM ferric nitrate in the buffer solution pH 3.7 at a scan rate of 50 mV/s.

swelling. Switching the pH up to 7.5 will flush out the unbound iron but increase Dopa complexation to the tris catecholate–Fe^{3+} mode, hence, condensing the films back to ~8 nm. There was no correlation between the mfp-1 (*Mc*) film thickness and the protein film deposition concentration (C_{fp1}) for different experiments; however, the measured trends in the adhesive/cohesive forces of interaction were consistent between experiments for similar deposition conditions.

Atomic Force Microscopy (AFM) Images. AFM was used to investigate the protein coverage on the mica surface for different C_{fp1}. Protein film deposited from a solution concentration of 10 μg/mL resulted in a partial coverage of the mica surface (Figure 4a,a′). At higher C_{fp1} of 50 and 100 μg/mL, the mica surface was completely covered with the protein film (Figure 4b,c,c′).

Cyclic Voltammetry (CV) on Mfp-1. CV measurements were performed on mfp-1 to investigate the oxidation behavior of the coating protein. Mfp-1 (*Mc*) showed an oxidation peak at E_O = 0.385 V corresponding to the oxidation of Dopa to Dopa–quinone. Dopa–quinone gets reduced back to Dopa reversibly at E_R = 0.310 V (Figure 5). Mfp-1 (*Me*), in contrast, exhibited Dopa with slightly lower redox stability at the same conditions (E_O = 0.365 V, E_R = 0.320 V). The differences in current (I) merely reflect the difference in total Dopa content in the two samples.

The current amplitude (I) of the oxidation peak current of mfp-1 (*Mc*) was decreased by approximately 60% when excess Fe^{3+} (10 μM) was added (Figure 5). This indicates that ~1/3 of the Dopa in mfp-1 (*Mc*) does not chelate iron and at pH 3.7 remains unbound in the protein even with excess Fe^{3+}. However, current for the Dopa mfp-1 (*Me*) decreased by ~90% following 10 μM Fe^{3+} addition, suggesting that nearly all the Dopa residues in mfp-1 (*Me*) chelate Fe^{3+} at pH 3.7 (Figure 5).

In Solution Fe^{3+} Binding by Dynamic Light Scattering (DLS). In solution, size comparisons of mfp-1 (*Me*) and mfp-1 (*Mc*) by DLS (Figure S2) showed similar size for mfp-1 (*Mc*; diameter, d = 35 nm, std. dev. 20 nm) and mfp-1 (*Me*; d = 41 nm, std. dev. 22 nm) aggregates in the absence of Fe^{3+} (Figure S2). Upon addition of excess iron, mfp-1 (*Me*) showed an increase in the peak intensity corresponding to the larger aggregate size (d ~ 277 nm), whereas mfp-1 (*Mc*) showed no change in size. However, the peak intensity corresponding to the smaller aggregate size increased upon the addition of iron to the mfp-1 (*Mc*) solution, suggesting that mfp-1 (*Mc*) monomers are stabilized by Fe^{3+}. The increase in the peak intensities of the larger aggregates in mfp-1 (*Me*)–iron solution is consistent with its tendency to form intermolecular Fe^{3+} bonds.

DISCUSSION

M. edulis (including the subspecies *M. galloprovincialis*) and *M. californianus* both make byssal threads coated with a hard energy-tolerant cuticle. That the toughness of *M. californianus* coating is much greater than that of *M. edulis* is due in large part to the former's greater breaking strain (~120% vs 75%). The coatings of both species are particle-filled composites; however, average particle diameters in *M. californianus* cuticle are less than a quarter of those in *M. edulis*. This is important because strain in both cuticles is enabled by microcracking at the interface between the matrix and particles. Because *M. californianus* affords 5× more particle surface area per unit

DOI: 10.1021/bm501893y
Biomacromolecules 2015, 16, 1002–1008

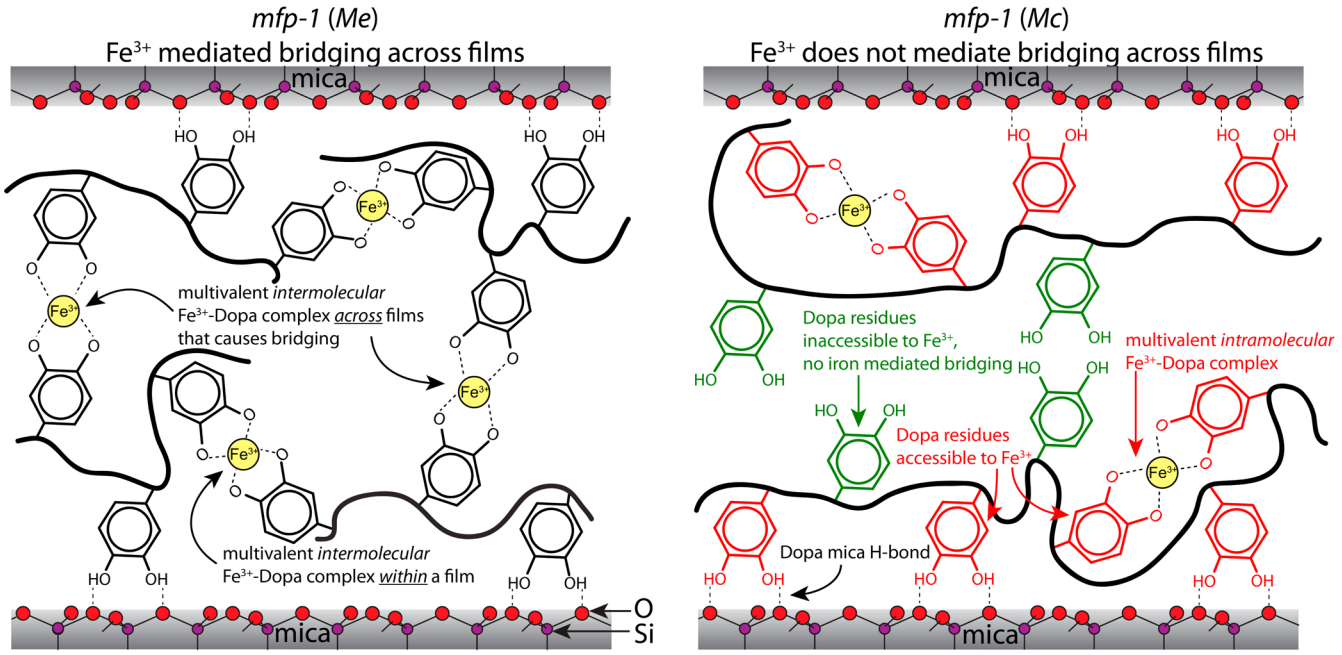

Figure 6. Molecular schematics of mfp-1 (*Me*) and mfp-1 (*Mc*) films on mica showing the interaction of the Dopa side chain with Fe^{3+} in the vicinity of the protein-mica binding site. The multivalent Fe^{3+}–Dopa complex is indicative of bis and tris modes of catecholato–Fe^{3+} coordination. The contribution of Lys and other amino acid residues is not shown in this figure. It should be noted that each mfp-1 molecule has ~100 Dopa residues and we present only a few of them to demonstrate the mechanism of metal chelation for the sake of clarity.

volume, more interfacial cracks can occur resulting in greater overall strain. Presented in this light, the overarching engineering question can be reduced to "how does *M. californianus* make smaller particles"?

As the particles or granules are enriched in Fe^{3+} and mfp-1 relative to the continuous matrix,[6] a reasonable hypothesis is that the assembly of mfp-1 in the two species into small or large granules is protein-templated. As established in the Introduction, molecular differences between the two mfp-1s seem slight: both consist of tandemly repeated decapeptides that are 80% identical and have a net change of only one amino acid side chain, that is, Ala (in *Me*) to Ile (in *Mc*). Conformation of the repeat decapeptide sequence has been investigated only for the *Me* sequence. A polyproline II or bent-helix has been proposed[40,41] in which Dopa-5 is less solvent-exposed than Dopa-9.[42] Dopa exposure is important for forming the *mono-*, *bis-*, and *tris*-catecholate complexes with Fe^{3+},[9] with a cumulative log stability of $K_s \sim 10$,[4543] thereby effectively cross-linking mfp-1.[6,15]

In contrast to previous SFA studies of mfps, we optimized conditions for mfp-1 (*Mc*) deposition from stock solutions (range 0–100 μg/mL) in order to obtain the highest adhesion or cohesion. Following these regimens, SFA testing of symmetric mfp-1 (*Mc*) films showed significant cohesion (up to −1.5 mJ/m^2) in contrast to mfp-1 (*Me*), which had little to no tendency for self-interaction at similar conditions.[15] As with other mfps, cohesion was compromised at pH 7.5 (due to Dopa oxidation); however, with added Fe^{3+}, intrinsic cohesion was maintained. Notably, the strong Fe^{3+}-mediated bridging of symmetric mfp-1 (*Mc*) films of the type associated with *Me* (W_c = 4 mJ/m^2) was absent. This absence persisted at all conditions tested for Fe^{3+} ($C_{Fe^{3+}}$ = 1–100 μM) and mfp-1 (*Mc*) C_{fp1} = 50–100 μg/mL (Figures S1 and S5).

Effective load bearing and load transfer between the opposing mfp-1 films on mica require both, strong cohesion between the two mfp-1 films and mfp-1 adhesion to mica. Generally speaking, at pH 5.5, mfp adhesion to mica is strong and attributed to electrostatic attraction between cationic amines (Lys) and surface siloxy anions as well as extensive bidentate hydrogen bonding between the Dopa and the polysiloxy mica surface.[37,38,44] The cohesion typically observed between symmetrically deposited mfp films is attributed to π-cation interactions between the positively charged Lys residues and the aromatic Dopa and Tyr groups as well as π–π interactions between the phenyl groups;[44−47] however, this cohesion is weak in symmetric mfp-1 (*Me*).[20] Perhaps, mfp-1 (*Me*) over-recruits Dopa groups to the mica surface, leaving only the Lys groups to face one another in repulsion.[20] Given the sequence similarity of mfp-1 in the two species this should be a cohesive problem for both proteins. As mfp-1 (*Mc*) has good cohesion and mfp-1 (*Me*) does not, the subtle sequence difference may result from fewer Dopa groups recruited to mica leaving more to contribute to cohesion in mfp-1 (*Mc*).

Effect of Fe^{3+} on the Cohesive Interactions between the Mfp-1 (*Mc*) Films. Most notably, Fe^{3+} addition ($C_{Fe^{3+}}$ = 1–100 μM) did not affect the cohesive energy measured between the mfp-1 (*Mc*) films deposited at C_{fp1} = 50–100 μg/mL (Figures S1 and S5). This is in stark contrast to the Fe^{3+} mediated bridging energy between two mfp-1 (*Me*) films at ~2–5 mJ/m^2 (Figure 3b).[15] DLS results (Figure S2) show that Fe^{3+} addition enhances aggregation in mfp-1 (*Me*), but not in mfp-1 (*Mc*). Cyclic voltammetry suggests that only half of the Dopa groups in mfp-1 (*Mc*) are engaged in forming catecholato–Fe^{3+} complexes at pH 3.7. At least 30–40% of the Dopa in mfp-1 (*Mc*) remains unbound and available for oxidation to Dopaquinone or coordinates Fe^{3+} only at higher pH. The latter is more probable. Dopa certainly occurs in two slightly different repeat sequences within mfp-1, that is, P*-S-Dopa-P for Dopa-5 and P*-T-Dopa-K for Dopa-9, but these are common to both *Me* and *Mc* homologues. The only evidence

DOI: 10.1021/bm501893y
Biomacromolecules 2015, 16, 1002–1008

for a functional difference between the two sequence motifs is that the 9-position is 2−3× more accessible enzymatic modification than the 5-position in mfp-1 (*Me*).[48]

The increased accessibility of Dopa-9, particularly as Dopa-Lys, is likely to be an important factor in mfp adhesion as measured by the SFA. More than half the Dopa in the strongly adhesive proteins, mfp-3f and mfp-5, has Lys or Arg groups flanking Dopa on one or both sides. If the same accessibility that helps Dopa chelate Fe^{3+} in mfp-1 (*Mc*) also helps binding to the mica crystal lattice, then, when a surface and Fe^{3+} are both present, there will be competition for accessible Dopa. In preadsorbing mfp-1 (*Mc*) to mica, many of the accessible Dopa residues are recruited to bind mica. Are the bound and unbound Dopa groups available for coordination to Fe^{3+}? According to resonance Raman spectroscopy (Figure S6), the shifts associated with Dopa−Fe^{3+} complexes have similar intensities in mfp-1 from both *Me* and *Mc*. Cyclic voltammetry, however, identifies distinct Dopa groups in mfp-1 (*Mc*) that do not bind iron (Figure 5). The contribution of the non-Fe^{3+} binding Dopa to cohesion between opposing mfp-1 (*Mc*) films must be significant.

It is now possible to model cohesive interactions with and without Fe^{3+} in mfp-1 for the two species (Figure 6). Without added Fe^{3+}, mfp-1 (*Mc*) has fewer Dopa groups recruited to the mica surface, so Dopa is available for H-bonding, π-cation, and $\pi-\pi$ interactions with the opposing face. With added Fe^{3+}, mfp-1 films of both species are endowed with extensive mono-, bis-, and tris-catecholate−Fe^{3+} complexes, however, these are primarily intermolecular in mfp-1 (*Me*) and intramolecular in mfp-1 (*Mc*; Figure 6). As a result, only mfp-1 (*Mc*) exhibits significant cohesive bridging without Fe^{3+}, whereas only mfp-1 (*Me*) has Fe^{3+}-mediated bridging in the presence of Fe^{3+}.

Taken together, the results suggest that although mfp-1s from both species complex Fe^{3+} (confirmed by resonance Raman analysis), mfp-1 (*Mc*) is better adapted to accumulate Fe^{3+} as a monomer, whereas mfp-1 (*Me*) aggregates as it accumulates Fe^{3+}. These differences in Fe^{3+} binding predict that symmetric films of mfp-1 (*Me*) in the SFA should show excellent bridging cohesion with Fe^{3+}, whereas mfp-1 (*Mc*) should not. The differences might also predict that granules made from mfp-1 (*Me*) would grow to a larger size that those from mfp-1 (*Mc*). Both predictions are realized.

In the presence of Fe^{3+}, each mfp-1 (*Mc*) molecule is inclined to collapse, whereas mfp-1 (*Me*) reaches out to share Fe^{3+} with other mfp-1 (*Me*)s. cDNA-deduced protein sequences of mfp-1 (*Mc*)[49] and mfp-1 (*Me*)[50] show that there is a subtle difference in the decapeptide repeat in the two proteins (see Supporting Information, Figure S8). The Ala → Ile substitution in the consensus decapeptide repeat of mfp-1 (*Mc*) could influence the accessibility of Dopa to Fe^{3+}. Possibly, the hydrophobic interaction between Ile-3 and Dopa-5 in mfp-1 (*Mc*) results in a different assembly. An intriguing biological consequence of this is that the granules in the *M. californianus* (*Mc*) byssal cuticle are much smaller (∼80%) than those in *M. edulis* (*Me* and its subspecies *Mg*)[5,51] and able to withstand almost twice the strain of those in *M. edulis*.[4,5]

CONCLUSIONS

Cohesive interactions between thin films of mfp-1 (*Mc*) were shown to depend strongly on the protein concentrations used for surface deposition and are maximal on mica at $C_{fp1} \sim 50$ μg/mL. Cohesion of mfp-1 revealed striking differences upon Fe^{3+} addition. For deposition of the protein at $C_{Fe^{3+}} = 0-100$ μM (pH 5.5), mfp-1 (*Mc*) films seem well adapted for intramolecular iron binding in contrast to the intermolecular binding of mfp-1 (*Me*). Iron stabilizes the bridging between the mfp-1 (*Mc*) films at pH 7.5, where most of the mussel foot proteins lose adhesion. The Lys residues flanking Dopa in mfp-1 sequences may be critical to determining the accessibility of Dopa for surface interactions and Fe^{3+} binding. Also the alanine (A) → isoleucine (I) substitution in the consensus decapeptide repeat may be responsible for creating two electrochemically distinct Dopa reactivities. Thus, metal chelation, with the right molecular architecture for a peptide chain can be used as a potential strategy to exploit mfp-1 mimetic biomacromolecules at physiological pH for wet adhesive applications.

ASSOCIATED CONTENT

Supporting Information

Cohesive and adhesive interactions between mfp-1 (*Mc* and *Me*) films; DLS, surface enhanced Raman spectroscopy measurements; XPS spectral deconvolution; Bradford assay; mfp-1 (*Mc*) film refractive index calculations. This material is available free of charge via the Internet at http://pubs.acs.org.

AUTHOR INFORMATION

Corresponding Authors

*E-mail: jacob@engineering.ucsb.edu. Phone: (805) 893-8407. Fax: (805) 893-7870.
*E-mail: waite@lifesci.ucsb.edu. Phone: (805) 893-2817.

Notes

The authors declare no competing financial interest.

ACKNOWLEDGMENTS

This research was supported by grants from NIH (R01 DE018468) and from the Institute for Collaborative Biotechnologies through Grant W911NF-09-0001 from the U.S. Army Research Office. The content of the information does not necessarily reflect the position or the policy of the Government, and no official endorsement should be inferred. This work was partially supported by the MRSEC Program of the National Science Foundation under Award No. DMR 1121053. Y.K. would like to thank the Otis Williams fellowship for their support.

REFERENCES

(1) Jacob, G. C.; Starbuck, J. M.; Fellers, J. F.; Simunovic, S.; Boeman, R. G. *J. Appl. Polym. Sci.* **2004**, *94*, 296−301.
(2) Jayabalan, M.; Lizymol, P. P.; Thomas, V. *Polym. Int.* **2000**, *49*, 88−92.
(3) Tjong, S. *Mater. Sci. Eng., R* **2006**, *53*, 73−197.
(4) Holten-Andersen, N.; Waite, J. H. *J. Dent. Res.* **2008**, *87*, 701−709.
(5) Holten-Andersen, N.; Zhao, H.; Waite, J. H. *Biochemistry* **2009**, *48*, 2752−2759.
(6) Harrington, M. J.; Masic, A.; Holten-Andersen, N.; Waite, J. H.; Fratzl, P. *Science* **2010**, *328*, 216−220.
(7) Sever, M. J.; Weisser, J. T.; Monahan, J.; Srinivasan, S.; Wilker, J. J. *Angew. Chem., Int. Ed.* **2004**, *43*, 448−450.
(8) Sun, C. J.; Waite, J. H. *J. Biol. Chem.* **2005**, *280*, 39332−39336.
(9) Taylor, S. W.; Chase, D. B.; Emptage, M. H.; Nelson, M. J.; Waite, J. H. *Inorg. Chem.* **1996**, *35*, 7572−7577.
(10) Monahan, J.; Wilker, J. J. *Chem. Commun.* **2003**, 1672−1673.
(11) Holten-Andersen, N.; Harrington, M. J.; Birkedal, H.; Lee, B. P.; Messersmith, P. B.; Lee, K. Y. C.; Waite, J. H. *Proc. Natl. Acad. Sci. U.S.A.* **2011**, *108*, 2651−2655.

DOI: 10.1021/bm501893y
Biomacromolecules 2015, 16, 1002−1008

(12) Ejima, H.; Richardson, J. J.; Liang, K.; Best, J. P.; van Koeverden, M. P.; Such, G. K.; Cui, J. W.; Caruso, F. *Science* **2013**, *341*, 154−157.
(13) Smith, J. J.; Thomson, A. J.; Proudfoot, A. E. I.; Wells, T. N. C. *Eur. J. Biochem.* **1997**, *244*, 325−333.
(14) Stewart, R. J.; Ransom, T. C.; Hlady, V. *J. Polym. Sci., Part B: Polym. Phys.* **2011**, *49*, 757−771.
(15) Zeng, H. B.; Hwang, D. S.; Israelachvili, J. N.; Waite, J. H. *Proc. Natl. Acad. Sci. U.S.A.* **2010**, *107*, 12850−12853.
(16) Tooney, N. M. *J. Polym. Sci., Polym. Lett. Ed.* **1980**, *18*, 643−644.
(17) Berglin, M.; Hedlund, J.; Fant, C.; Elwing, H. *J. Adhes.* **2005**, *81*, 805−822.
(18) Inoue, K.; Odo, S. *Biol. Bull.* **1994**, *186*, 349−355.
(19) Waite, J. H.; Tanzer, M. L. *Science* **1981**, *212*, 1038−1040.
(20) Lin, Q.; Gourdon, D.; Sun, C. J.; Holten-Andersen, N.; Anderson, T. H.; Waite, J. H.; Israelachvili, J. N. *Proc. Natl. Acad. Sci. U.S.A.* **2007**, *104*, 3782−3786.
(21) Rodriguez, N. R. M.; Das, S.; Kaufman, Y.; Wei, W.; Israelachvili, J.; Waite, J. H. *Biomaterials* **2015**, *51*, 51−57.
(22) Das, S.; Cadirov, N.; Chary, S.; Kaufman, Y.; Hogan, J.; Turner, K. L.; Israelachvili, J. N. *J. R. Soc., Interface* **2015**, *12*, 20141346.
(23) Pogula, S. D.; Patwardhan, S. V.; Perry, C. C.; Gillespie, J. W.; Yarlagadda, S.; Kiick, K. L. *Langmuir* **2007**, *23*, 6677−6683.
(24) Fichman, G.; Adler-Abramovich, L.; Manohar, S.; Mironi-Harpaz, I.; Guterman, T.; Seliktar, D.; Messersmith, P. B.; Gazit, E. *ACS Nano* **2014**, *8*, 7220−7228.
(25) Das, S.; Banquy, X.; Zappone, B.; Greene, G. W.; Jay, G. D.; Israelachvili, J. N. *Biomacromolecules* **2013**, *14*, 1669−1677.
(26) Zhao, H.; Waite, J. H. *J. Biol. Chem.* **2006**, *281*, 26150−26158.
(27) Waite, J. H.; Benedict, C. V. *Methods Enzymol.* **1984**, *107*, 397−413.
(28) Inoue, K.; Waite, J. H.; Matsuoka, M.; Odo, S.; Harayama, S. *Biol. Bull.* **1995**, *189*, 370−375.
(29) Väinölä, R.; Hvilsom, M. *Biol. J. Linn. Soc.* **1991**, *43*, 127−148.
(30) Rawson, P. D.; Agrawal, V.; Hilbish, T. J. *Mar. Biol.* **1999**, *134*, 201−211.
(31) Lucas, J. M.; Vaccaro, E.; Waite, J. H. *J. Exp. Biol.* **2002**, *205*, 1807−1817.
(32) Das, S.; Donaldson, S. H., Jr; Kaufman, Y.; Israelachvili, J. N. *RSC Adv.* **2013**, *3*, 20405−20411.
(33) Israelachvili, J.; Min, Y.; Akbulut, M.; Alig, A.; Carver, G.; Greene, W.; Kristiansen, K.; Meyer, E.; Pesika, N.; Rosenberg, K.; Zeng, H. *Rep. Prog. Phys.* **2010**, *73*, 036601−036617.
(34) Das, S.; Chary, S.; Yu, J.; Tamelier, J.; Turner, K. L.; Israelachvili, J. N. *Langmuir* **2013**, *29*, 15006−15012.
(35) Israelachvili, J. N. *Intermolecular and Surface Forces*, 3rd ed.; Academic Press: New York, 2011; pp 1−674.
(36) Israelachvili, J. N.; Kristiansen, K.; Gebbie, M. A.; Lee, D. W.; Donaldson, S. H.; Das, S.; Rapp, M. V.; Banquy, X.; Valtiner, M.; Yu, J. *J. Phys. Chem. B* **2013**, *117*, 16369−16387.
(37) Anderson, T. H.; Yu, J.; Estrada, A.; Hammer, M. U.; Waite, J. H.; Israelachvili, J. N. *Adv. Funct. Mater.* **2010**, *20*, 4196−4205.
(38) Anderson, T.; Israelachvili, J. *Biophys. J.* **2010**, *98*, 594a−594a.
(39) Gieseg, S. P.; Simpson, J. A.; Charlton, T. S.; Duncan, M. W.; Dean, R. T. *Biochemistry* **1993**, *32*, 4780−4786.
(40) Kanyalkar, M.; Srivastava, S.; Coutinho, E. *Biomaterials* **2002**, *23*, 389−396.
(41) Haemers, S.; van der Leeden, M. C.; Frens, G. *Biomaterials* **2005**, *26*, 1231−1236.
(42) Williams, T.; Marumo, K.; Waite, J. H.; Henkens, R. W. *Arch. Biochem. Biophys.* **1989**, *269*, 415−422.
(43) Taylor, S. W.; Waite, J. H.; Ross, M. M.; Shabanowitz, J.; Hunt, D. F. *J. Am. Chem. Soc.* **1994**, *116*, 10803−10804.
(44) Nicklisch, S. C. T.; Das, S.; Rodriguez, N. R. M.; Waite, J. H.; Israelachvili, J. N. *Biotechnol. Prog.* **2013**, *29*, 1587−1593.
(45) Greene, G. W.; Lee, D. W.; Yu, J.; Das, S.; Banquy, X.; Israelachvili, J. N. Lubrication and Wear Protection of Natural (Bio)Systems. *Polymer Adhesion, Friction, and Lubrication*; John Wiley & Sons, Inc.: New York, 2013; pp 83−133.
(46) Kearney, P. C.; Mizoue, L. S.; Kumpf, R. A.; Forman, J. E.; Mccurdy, A.; Dougherty, D. A. *J. Am. Chem. Soc.* **1993**, *115*, 9907−9919.
(47) Pillai, K. V.; Renneckar, S. *Biomacromolecules* **2009**, *10*, 798−804.
(48) Marumo, K.; Waite, J. H. *Biochim. Biophys. Acta* **1986**, *872*, 98−103.
(49) Waite, J. H. *J. Comp. Physiol., B* **1986**, *156*, 491−496.
(50) Filpula, D. R.; Lee, S. M.; Link, R. P.; Strausberg, S. L.; Strausberg, R. L. *Biotechnol. Prog.* **1990**, *6*, 171−177.
(51) Harrington, M. J.; Waite, J. H. *J. Exp. Biol.* **2007**, *210*, 4307−4318.

DOI: 10.1021/bm501893y
Biomacromolecules 2015, 16, 1002−1008